

Supporting Online Material for **800,000 Years of Abrupt Climate Variability**

Stephen Barker,* Gregor Knorr, R. Lawrence Edwards, Frédéric Parrenin, Aaron E. Putnam,
Luke C. Skinner, Eric Wolff, Martin Ziegler

*To whom correspondence should be addressed. E-mail: barkers3@cf.ac.uk

Published 8 September 2011 on *Science* Express
DOI: 10.1126/science.1203580

This PDF file includes:

Materials and Methods

Figs. S1 to S14

Table S1

References

Additional material includes the following:

Tables S2 and S3

800,000 years of abrupt climate variability

Stephen Barker, Gregor Knorr, R. Lawrence Edwards, Frédéric Parrenin, Aaron E. Putnam, Luke C. Skinner, Eric Wolff and Martin Ziegler

Supporting Online Material

The US National Research Council Committee on Abrupt Climate Change (*1*) defines an abrupt climate change as one that occurs when the climate system is forced to cross some threshold, triggering a transition to a new state at a rate determined by the climate system itself and faster than the cause.

Smoothing records and removing orbital-timescale variability

All smoothing is performed by applying a running mean (of the length specified) twice to the evenly sampled datasets. Removal of orbital-timescale variability is achieved by subtracting a 7 kyr smooth.

Smoothing of the Antarctic temperature record its derivative

Before taking the first derivative of AA_T we remove orbital-timescale variability to give AA_{T_hi} , in order to remove ambiguities resulting from the superposition of millennial-scale events on orbital-timescale variations (Fig. S1). Since the changes we are interested in (abrupt warming events in Greenland) appear as short-lived minima in the record of AA_T'' we do not need to apply this treatment to the original temperature record (even before taking the first differential) for deriving the second differential. This is demonstrated by the similarity between the records of AA_T'' with and without removal of the 7 kyr smooth (Fig. S1). Although it makes little difference we choose not to remove orbital-timescale variability before deriving the second differential in order to minimise the number of processing steps involved in our analysis.

The act of differentiating (by finite differences) amplifies noise in the original record and it is therefore necessary to smooth this record before differentiating. However, the choice of smoothing window length is a trade-off between loss of unwanted noise and loss in the signal we wish to isolate. These effects can be observed by comparing records of AA_{T_hi}' produced after smoothing AA_T with various window lengths, and their correlation with GL_{T_hi} (Fig. S2). We suggest that a smoothing window of 700 years provides a reasonable compromise between noise reduction and signal fidelity. This is comparable to the running mean window applied by the study of (2).

Selecting events when the first derivative (AA_{T_hi}') decreases through zero (which would coincide with abrupt warming events in Greenland, according to the seesaw model) provides another means to assess the effect of different smoothing window length (Fig. S3). We note that low order smoothing (200-300 yr) predicts many events that do not have obvious correlatives in Greenland while high order (1000 yr) smoothing results in loss of events. We also smooth the record of AA_T' before differentiating a second time in order to analyse minima in AA_T'' (Fig. S3). Critically we note that the timing of significant minima in AA_T'' (used to identify D-O warming events) is not particularly sensitive to the choice of filter length. We apply a 700 yr smooth to AA_T' before differentiating a second time to produce AA_T'' . We note that a longer smoothing window results in loss of events.

GL_T versus AA_T' and the effect of uncertainty in Δage

In order to compare the phasing between temperature records from Greenland and Antarctica we rely on the methane tuning method developed by Blunier and Brook (3, 4). By making the assumption that changes in atmospheric CH₄ will be essentially contemporaneous in both hemispheres it is possible to place the gas records from disparate locations on a common timescale. In order to place the corresponding temperature records (which are most commonly derived from the ice phase) on the same common timescale, it is necessary to know the age offset (Δ age) between the ice and trapped gas at any depth within the core (the gas will always be younger than the surrounding ice because the circulation of gas within the firn is only stopped once the ice is compacted). Unfortunately the uncertainty in the age offset is considerable (up to hundreds of years). Therefore we are unable to determine the precise phase relationships between the records derived from ice to better than ~200 years based on this method. As shown in the main text Figure 1, the approximate out-of-phase relationship between GL_T_hi and AA_T_hi' actually suggests a small (100-150 yr) lead of Greenland over Antarctica. However, when we perform the same analysis on the GISP (Greenland) and Byrd (Antarctica) temperature records (as aligned by (4)) we find that AA_T_hi' leads GL_T_hi by ~200 years (Fig. S4). We suggest that these differences result from the uncertainties in Δ age and argue that the true relationship should be antiphase. Our findings appear to resolve the discussion between (5), (6) and (7) who were essentially describing the differences between GL_T_hi versus AA_T_hi and GL_T_hi versus AA_T_hi'.

Construction of “GL_T_syn”

To produce a reconstruction of Greenland temperature variability (Fig. S5) from the EDC δD record (8) we first apply a 7000 year smooth to the Antarctic record to produce AA_T_lo. We then subtract AA_T_lo from AA_T and smooth the result at 700 year to produce AA_T_hi. This is differentiated to produce AA_T_hi'. We then normalise AA_T_hi' (divide through by its own standard deviation) and scale it to the record of GL_T_hi by multiplying the normalised record of AA_T_hi' by the standard deviation of GL_T_hi. This produces GL_T_syn_hi. We produce GL_T_syn_lo by scaling the record of AA_T_lo to GL_T_lo (by normalising and applying the same mean and standard deviation) and shifting it towards younger ages by 2000 years (see next paragraph). GL_T_syn is then the sum of GL_T_syn_hi and GL_T_syn_lo.

The thermal bipolar seesaw model was constructed to explain millennial-scale oscillations during the last glacial period. However, the temperature records from Greenland ice cores include longer-term variations (so-called orbital-timescale variability). We wish to produce a reconstruction of what Greenland temperature records might look like if they extended back as far as those from Antarctica. This requires us to add orbital-timescale variability to our record of GL_T_syn_hi. The orbital-timescale component of the Antarctic temperature record (AA_T_lo) is highly correlated with GL_T_lo over the last 100 kyr (9) (Figs. S5, S6). Furthermore, both signals appear correlated to variations in northern hemisphere summer insolation (10-13). While the link between the northern temperature record and northern summer insolation may be comparatively straightforward (through direct effects such as ice albedo), the correlation between northern summer insolation and southern temperature records is less obvious (13). Explanations have most often argued that northern hemisphere insolation must provide an indirect forcing on southern hemisphere temperatures (through e.g. CO₂ or ocean circulation changes) (14, 15) although a recent study suggests that southern insolation itself may be responsible via the influence of summer duration (which is in phase with northern hemisphere summer intensity) as opposed to intensity (12). Whatever the explanation, the correlation holds for at least the last 800,000 years (8). Atmospheric CO₂ concentrations may also play a role in the interhemispheric symmetry of the temperature records on

longer timescales. Although changes in CO₂ typically lag temperature changes over Antarctica by several hundreds of years on multi-millennial timescales (16) CO₂ probably plays a role in the amplitude of these changes (for example it may help to explain the amplitude of glacial-interglacial changes). Given the observed similarity between the low frequency components of the Greenland and Antarctic records over the last 100 kyr, we suggest that the record of AA_T_lo represents a reasonable substitute for GL_T_lo in our reconstruction of Greenland temperature variability.

The record of AA_T_lo appears to lead that of GL_T_lo by around 2000 years (9) although the precise lag is difficult to determine given the length of the records (Figs. S5, S6). This may be due to *e.g.* the slow response of northern hemisphere ice sheets to insolation forcing or it may reflect the pervasive influence of millennial-scale oscillations on the Antarctic record (for example during late MIS 4 (HS6), when Greenland was cold, Antarctica warmed, possibly through the seesaw mechanism. This would give rise to an apparent lead of Antarctic over Greenland on longer timescales). When the record of AA_T_lo is scaled to GL_T_lo (same mean and standard deviation) the offset between the two records (Fig. S5F) is typically less than 1‰. This offset can be reduced by shifting GL_T_syn_lo by 2000 years to provide a better match with GL_T_lo. The offset is relatively small compared to the high amplitude of D-O oscillations (typically 3-4‰) and to the overall magnitude of glacial-interglacial variability. Furthermore the offset changes slowly with respect to the abruptness of D-O events. We therefore include a shift of 2000 years in GL_T_syn_lo. When we include GL_T_syn_lo in our reconstruction of GL_T_syn we achieve a reasonable result (Fig. 2G).

We chose the EDC δD record for our construction of GL_T_syn because it is the longest published record and we compared our results with the GISP ice core because this allows straightforward derivation a common age scale via CH₄ tuning (Fig. 1). For completeness we show a comparison of the first differentials of EDC, EDML (both normalised) and a composite Antarctic record (derived by tuning and normalising the isotope records from EDC (8), EDML (17), Vostok (11), Dome Fuji (18) and Byrd (19)) with the millennial-scale components of the GISP (20) and NGRIP (21) ice cores (Fig. S7).

Synthetic records are given in Table S2.

Prediction of ‘D-O-type’ events using the Antarctic record

We employ a thresholding approach for predicting the occurrence of abrupt Greenland warming events based on minima in the second time differential of AA_T (AA_T‘‘) (Fig. 2E, F). This has an advantage over use of the first differential (decreasing through zero) because it is capable of distinguishing between events of varying magnitude and incorporates information about conditions before and after an abrupt event. For example, the large D-O events, 19 and 20, were characterised by a rapid transition from pronounced warming to equally pronounced cooling over Antarctica (Fig. 2). This information is captured by the exaggerated minima in AA_T‘‘, which may then reflect particularly significant changes in the AMOC and related atmospheric phenomena associated with these events. If a minimum in AA_T‘‘ exceeds a threshold, an event is generated and assigned the age of that minimum (Fig. 2E). Using a relatively insensitive threshold (blue dashed line in Fig. 2F) we are able to identify the largest D-O temperature shifts recorded in Greenland while ‘smaller’ events, such as D-O 2, require a more sensitive threshold (red line). Based on this we are able to identify almost all of the canonical D-O events over the last 90 kyr without introducing ‘spurious events’.

Correcting for signal loss due to sample time integration

Before applying our two approaches for reconstructing Greenland climate to the full 800 kyr record of AA_T (*i.e.* δD) from the EDC ice core we need to investigate the possible effects of ice flow and diffusion in the deeper parts of the record. Both of these processes may result in a reduction in the amplitude of variability in δD (either through diffusion (22, 23)) or simply because the sampling for δD measurements (made on 55cm sections of ice) tends to integrate longer time intervals for deeper parts of the core. For example, within the upper few meters of the EDC ice core each 55cm sample represents < 10 years of ice accumulation whereas at 3042m (~640 ka) a 55cm sample integrates >1350 years of ice (Fig. S8a). It has also recently been argued that diffusion length scales may reach up to 40cm for the deepest parts of the EDC ice core (23). Since this is of the same order as the sampling window we address both issues together. We do so by constructing a synthetic Antarctic ice core temperature record (Syn AA_T) (Fig. S8) and use this to investigate the potential effects of fidelity loss in deeper parts of the record. We start by assuming that the real EDC ice core temperature record for the last 100 kyr or so represents actual temperature variations over Antarctica (*i.e.* without significant signal attenuation on millennial-timescales). We then select a 100 kyr interval with similar δD values at either end (in this case ~12 to ~112 ka) and produce a synthetic history of temperature for 800 kyr by repeating this interval 8 times. Finally we ‘sample’ this synthetic temperature history in the same manner as the actual EDC ice core record samples the real temperature history over Antarctica (by integrating the same time intervals as each 55cm sample does for the real record).

The loss of signal amplitude is immediately apparent for deeper sections of the synthetic record (Fig. S8A). The corresponding ‘loss’ of predicted D-O events, based on minima in AA_T'' below a fixed threshold, is significant. We address this by allowing the picking threshold to vary according to the time integrated by each 55cm of ice (Fig. S8A). We apply the simplest approach for incorporating the ‘time-per-sample’ factor into our D-O prediction algorithm. For adjusting the threshold used to pick D-O events based on minima in AA_T'' , we ratio the corresponding time-per-sample to the minimum value for this parameter (5.81 yr), scale it (divide by 2.3×10^7) and add it to a baseline threshold (-1×10^{-5}) (Fig. S8A, B). This operation effectively accounts for smoothing of the record by exaggerating the minima in AA_T'' with respect to the threshold. Use of the variable threshold recovers most of the D-O events that were lost using the fixed threshold approach (Fig. S8C). The choice of parameters for the thresholding exercise was based on a trade-off between picking as many canonical D-O events as possible while minimising the number of predicted events with no obvious analogy in Greenland. Thus some canonical events are not picked (*e.g.* events 2 and 9). We note that for sections of the record where the time-integrated-per-sample approaches or exceeds 1000 years (~600-800 ka) two individual millennial-scale events may be merged into a single event, which our variable threshold cannot account for. Therefore, while we are confident that our approach does not predict a significant number of spurious events, we must acknowledge that some events may be lost altogether.

We could use a similar approach to adjust the amplitude of variability observed in the record of $\text{AA}_T\text{-hi}'$ (and therefore in $\text{GL}_T\text{-syn-hi}'$). However, the long-lived nature of some Antarctic warming and cooling events (especially those associated with glacial terminals) means that in these cases the increase in sample time integration does not impact the first differential to a significant degree (Fig. S9). Correcting for signal attenuation would therefore result in a spurious amplification of the $\text{AA}_T\text{-hi}'$ record in certain places and we choose not to apply an adjustment to $\text{GL}_T\text{-syn}$. It must be acknowledged therefore that as well as the total loss of very short events, the amplitude of shorter events (~1-2 kyr) in the oldest portion of $\text{GL}_T\text{-syn}$ (600-800 ka) will be reduced relative to the actual Greenland events they correspond with.

Picked D-O events are given in Table S3.

The Chinese speleothem record

In order to assess the millennial-scale variability within the Chinese speleothem record we need to remove the orbital-scale variations, which mirror July insolation at 65°N (24) (Fig. S10) (we note that there is currently some discussion about the precise insolation target that should be used (25, 26) but choose that which is in-phase with the orbitally-filtered speleothem record). We achieve this by removing the normalised (by subtracting its mean and dividing through by its standard deviation) insolation curve from the normalised speleothem record (Fig. S10). Before normalisation, the individual speleothem records require some adjustment to align them to a common scale. This is achieved by subtracting 1.6 from the Hulu Cave records to account for the difference in elevation and location between the various cave sites (24).

Derivation of absolute timescales

Thanks to the near one-to-one correspondence between ‘weak monsoon events’ in the detrended speleothem record and cold events in our synthetic records, GL_T_syn_hi and GL_T_syn (main text Fig. 3) we are able to align these events in order to place the EDC records on the absolute ‘Speleo-Age’ timescale (Fig. S11A, S12). Uncertainties in resultant age model (‘Speleo-Age’) arise from uncertainties in the absolute dating of the speleothem record (dating error) and the fact that ‘abrupt’ transitions in both records (GL_T_syn and speleothem $\delta^{18}\text{O}$) sometimes appear to last up to hundreds of years (tuning error). We provide estimates of these errors with their corresponding tie points in Table S1. It is clear that this exercise will improve as more speleothem records are produced and as dating methods improve. For now we do not attempt alignment where the speleothem record has insufficient resolution to allow recognition of abrupt events (*i.e.* the interval 315–265 ka). In general the resultant offset between our absolute timescale for EDC and the published EDC3 age model (27) is of the order 0–1000 years with some events shifted by ~3000 yr and up to 5000 yr toward the oldest part of the speleothem record (Table S1). These estimates are within the age uncertainties of the EDC3 age model (27). These offsets are also similar in magnitude to our estimate of the total uncertainty in our absolute age model although our revised age model in general shifts the record toward older ages.

Our revised age model for the EDC records is fundamentally based on the EDC3 age model and should be considered a refinement of that. From here we derive absolute timescales for the records from ODP 980 in the North Atlantic (28) (Fig. S11B, S13) and MD01-2444 and MD01-2443 from the Iberian Margin (29) (Fig. S11C; S14).

We note good correspondence between our absolute age model and the results of Drysdale *et al.* (30) for Termination II. We derive an age of 129.6 ± 0.7 ka for the end of Heinrich event 11. This compares with 129 ± 1.5 ka by (30).

Supplementary references.

1. National Research Council, Committee on Abrupt Climate Change, *Abrupt Climate Change: Inevitable Surprises*. (The National Academies Press, Washington DC, 2002).
2. B. Stenni *et al.*, The deuterium excess records of EPICA Dome C and Dronning Maud Land ice cores (East Antarctica). *Quat. Sci. Rev.* **29**, 146 (2010).
3. T. Blunier *et al.*, Asynchrony of Antarctic and Greenland climate change during the last glacial period. *Nature* **394**, 739 (1998).
4. T. Blunier, E. J. Brook, Timing of millennial-scale climate change in Antarctica and Greenland during the last glacial period. *Science* **291**, 109 (2001).
5. A. Schmittner, O. A. Saenko, A. J. Weaver, Coupling of the hemispheres in observations and simulations of glacial climate change. *Quat. Sci. Rev.* **22**, 659 (2003).
6. P. Huybers, Comments on 'Coupling of the hemispheres in observations and simulations of glacial climate change' by A. Schmittner, O.A. Saenko, and A.J. Weaver. *Quat. Sci. Rev.* **23**, 207 (2004).
7. A. Schmittner, O. A. Saenko, A. J. Weaver, Response to the comments by Peter Huybers. *Quat. Sci. Rev.* **23**, 210 (2004).
8. J. Jouzel *et al.*, Orbital and millennial Antarctic climate variability over the past 800,000 years. *Science* **317**, 793 (2007).
9. C. Wunsch, Greenland - Antarctic phase relations and millennial time-scale climate fluctuations in the Greenland ice-cores. *Quat. Sci. Rev.* **22**, 1631 (2003).
10. W. Dansgaard *et al.*, Evidence for General Instability of Past Climate from a 250-Kyr Ice-Core Record. *Nature* **364**, 218 (1993).
11. J. R. Petit *et al.*, Climate and atmospheric history of the past 420,000 years from the Vostok ice core, Antarctica. *Nature* **399**, 429 (1999).
12. P. Huybers, G. Denton, Antarctic temperature at orbital timescales controlled by local summer duration. *Nature Geoscience* **1**, 787 (2008).
13. P. Huybers, Antarctica's Orbital Beat. *Science* **325**, 1085 (2009).
14. R. B. Alley, E. J. Brook, S. Anandakrishnan, A northern lead in the orbital band: north-south phasing of Ice-Age events. *Quat. Sci. Rev.* **21**, 431 (2002).
15. J. Imbrie *et al.*, On the structure and origin of major glaciation cycles 2. the 100,000-year cycle. *Paleoceanography* **8**, 699 (1993).
16. J. Ahn, E. Brook, Atmospheric CO₂ and climate from 65 to 30 ka B.P. *Geophys. Res. Lett.* **34**, doi:10.1029/2007GL029551 (2007).
17. EPICA, One-to-one coupling of glacial climate variability in Greenland and Antarctica. *Nature* **444**, 195 (2006).
18. K. Kawamura *et al.*, Northern Hemisphere forcing of climatic cycles in Antarctica over the past 360,000 years. *Nature* **448**, 912 (2007).
19. S. J. Johnsen, H. B. Clausen, Dansgaard.W, C. C. Langway, Oxygen Isotope Profiles through Antarctic and Greenland Ice Sheets. *Nature* **235**, 429 (1972).
20. M. Stuiver, P. M. Grootes, GISP2 oxygen isotope ratios. *Quat. Res.* **53**, 277 (2000).
21. NGRIP_members, High-resolution record of Northern Hemisphere climate extending into the last interglacial period. *Nature* **431**, 147 (2004).
22. S. J. Johnsen, Stable isotope homogenization of polar firn and ice. in *Isotopes and Impurities in Snow and Ice*. (IAHS, Grenoble, 1977), vol. 11B, pp. 210-219.
23. K. Pol *et al.*, New MIS 19 EPICA Dome C high resolution deuterium data: Hints for a problematic preservation of climate variability at sub-millennial scale in the "oldest ice". *Earth Planet. Sci. Lett.* **298**, 95 (2010).
24. Y. J. Wang *et al.*, Millennial- and orbital-scale changes in the East Asian monsoon over the past 224,000 years. *Nature* **451**, 1090 (2008).

25. S. C. Clemens, W. L. Prell, Y. B. Sun, Orbital-scale timing and mechanisms driving Late Pleistocene Indo-Asian summer monsoons: Reinterpreting cave speleothem delta O-18. *Paleoceanography* **25**, (2010).
26. M. Ziegler, E. Tuenter, L. J. Lourens, The precession phase of the boreal summer monsoon as viewed from the eastern Mediterranean (ODP Site 968). *Quat. Sci. Rev.* **29**, 1481 (2010).
27. F. Parrenin *et al.*, The EDC3 chronology for the EPICA dome C ice core. *Climate of the Past* **3**, 485 (2007).
28. J. F. McManus, D. W. Oppo, J. L. Cullen, A 0.5-million-year record of millennial-scale climate variability in the North Atlantic. *Science* **283**, 971 (1999).
29. B. Martrat *et al.*, Four climate cycles of recurring deep and surface water destabilizations on the Iberian margin. *Science* **317**, 502 (2007).
30. R. N. Drysdale *et al.*, Evidence for Obliquity Forcing of Glacial Termination II. *Science* **325**, 1527 (2009).
31. Y. J. Wang *et al.*, A high-resolution absolute-dated Late Pleistocene monsoon record from Hulu Cave, China. *Science* **294**, 2345 (2001).
32. H. Cheng *et al.*, Ice Age Terminations. *Science* **326**, 248 (2009).
33. E. J. Steig, R. B. Alley, Phase relationships between Antarctic and Greenland climate records. *Annals of Glaciology* **35**, 451 (2002).
34. A. Berger, M. F. Loutre, Insolation Values for the Climate of the Last 10 Million Years. *Quat. Sci. Rev.* **10**, 297 (1991).
35. L. E. Lisiecki, M. E. Raymo, A Pliocene-Pleistocene stack of 57 globally distributed benthic $\delta^{18}\text{O}$ records. *Paleoceanography* **20**, PA1003 (2005).

Supplementary figures

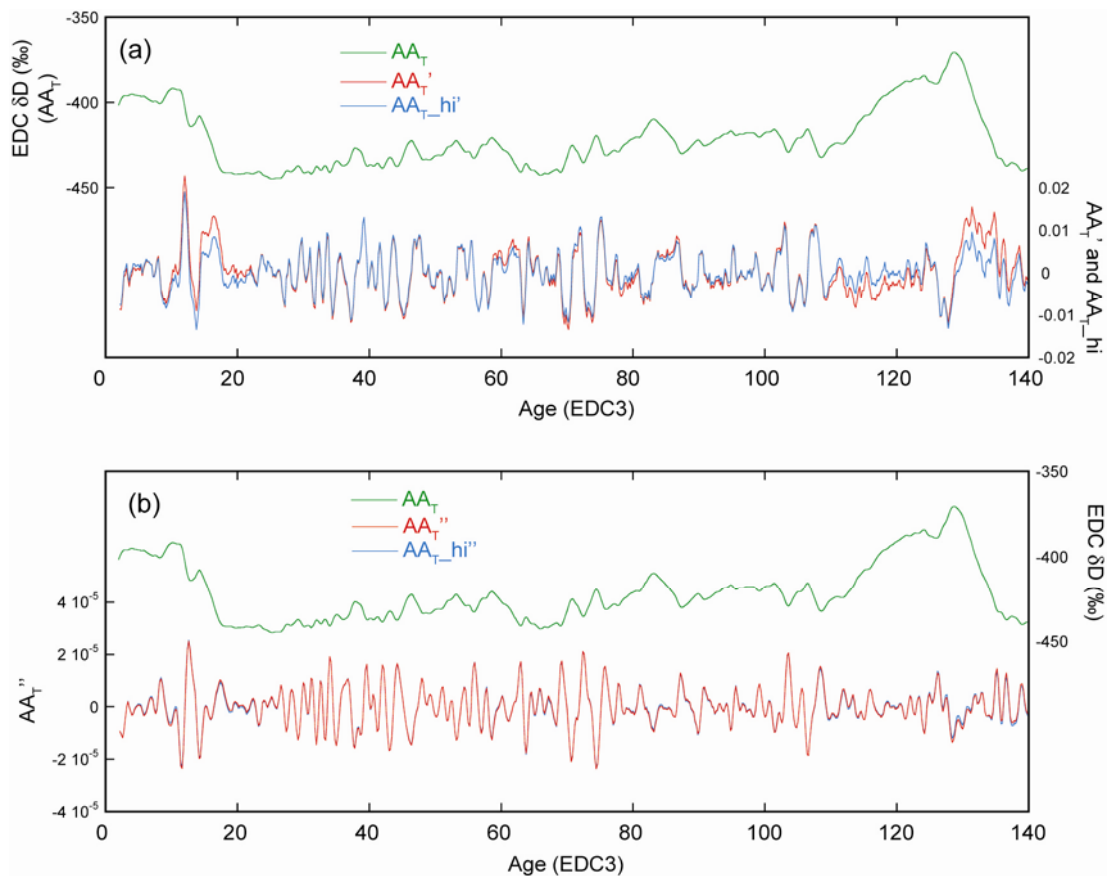


Figure S1. Effect of high-pass filtering on AA_T' and AA_T'' . (a) The first differential (AA_T') is sensitive to the interplay between millennial- and orbital-timescale variations. The corresponding effect on the second differential (b) is minimal.

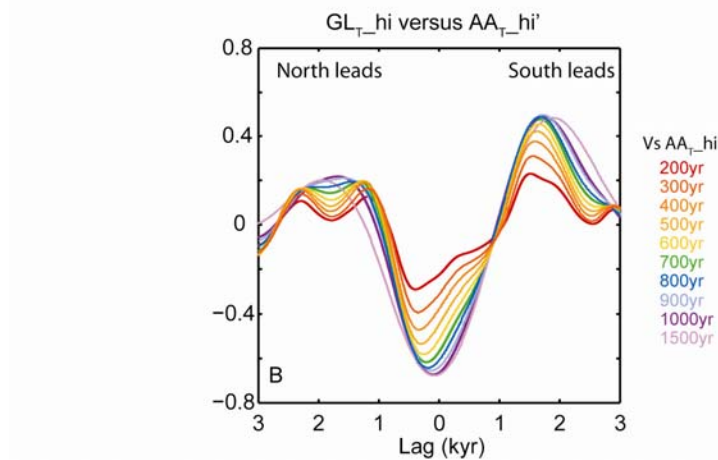
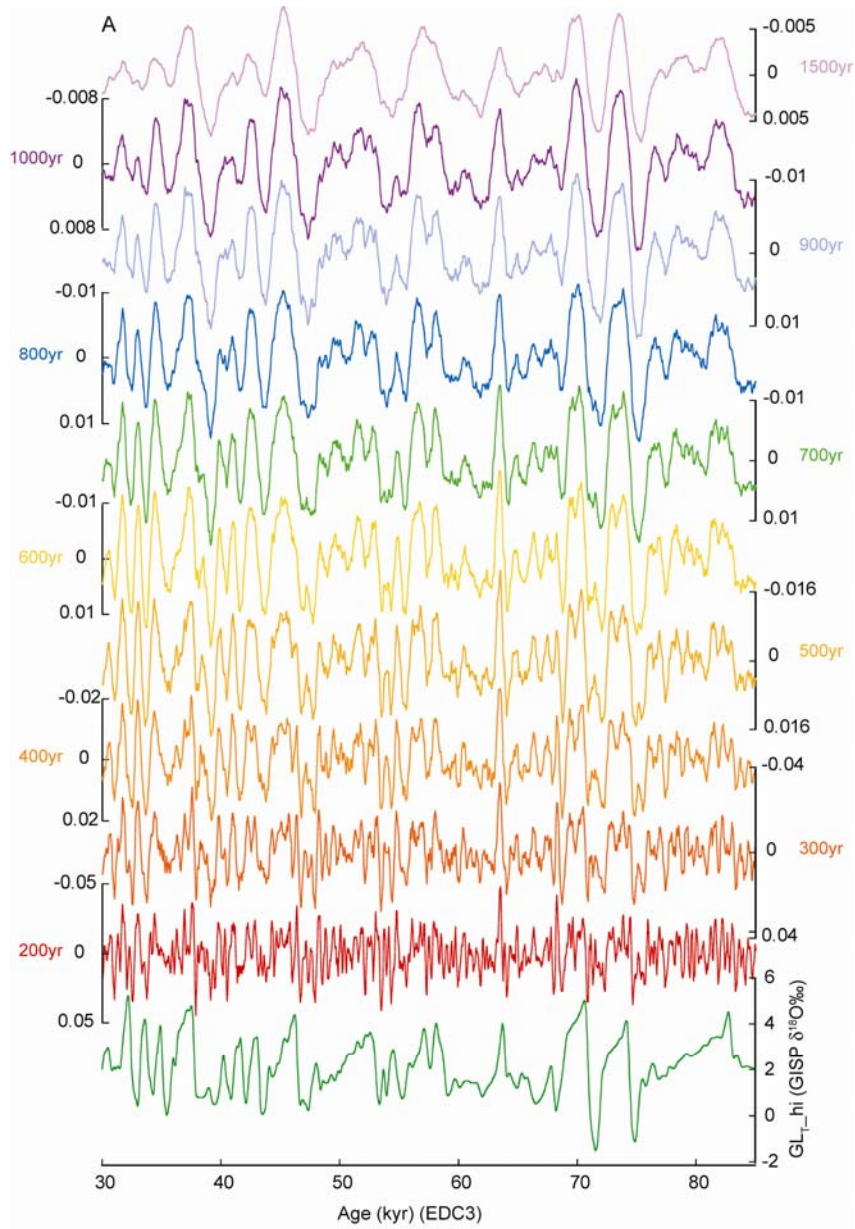
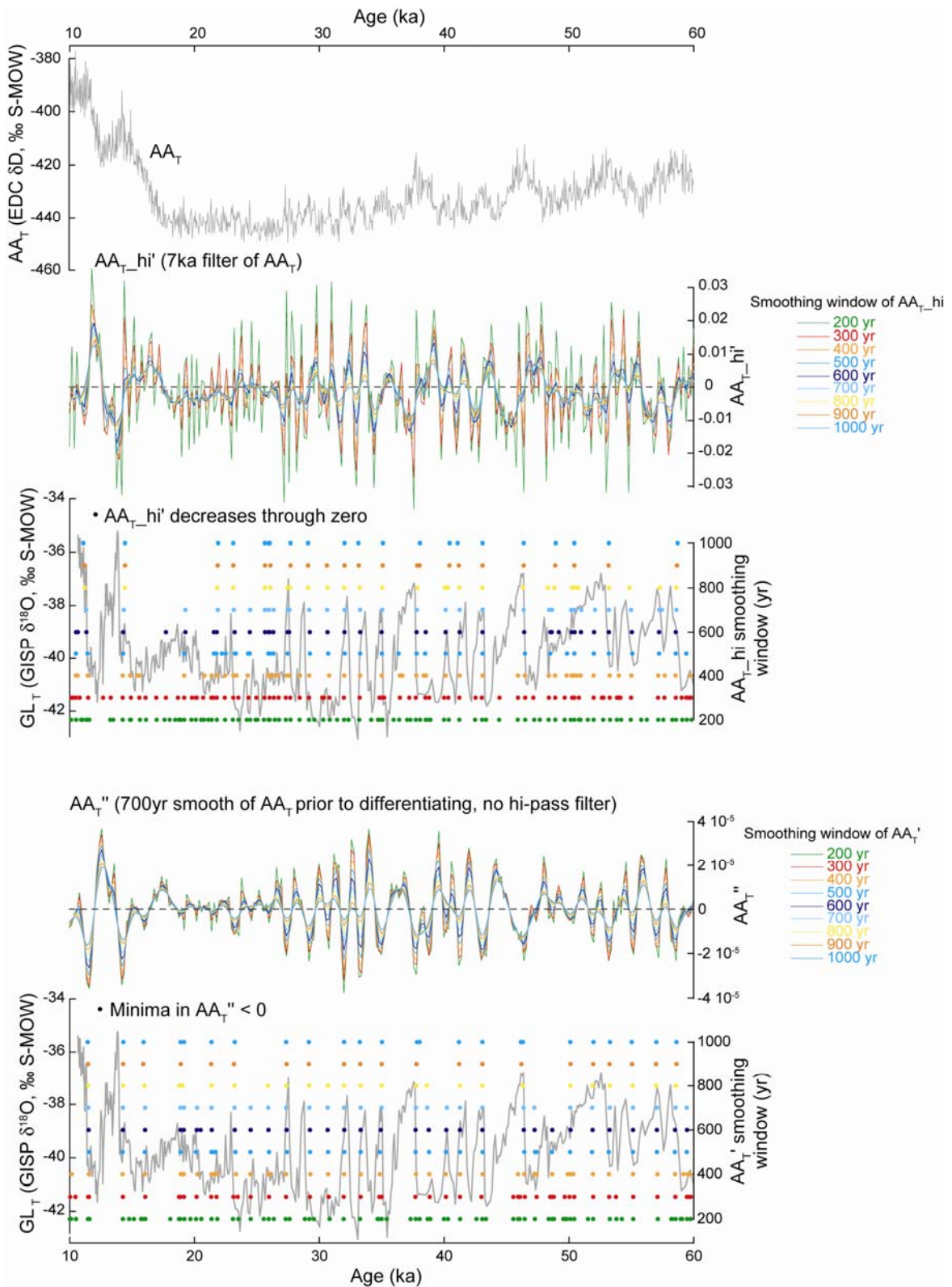


Figure S2. Smoothing of $\text{AA}_{\text{T}}\text{-hi}$ before differentiating causes a reduction in noise but results in a reduction in the abruptness of predicted events as compared with the Greenland record. The choice of 700 years for the filter length is made based on compromise between optimal correlation between $\text{AA}_{\text{T}}\text{-hi}'$ and $\text{GL}_{\text{T}}\text{-hi}$ and the obliteration of certain features in the record (see also Fig. S3).



GISP versus Byrd (BB01)
85-30 ka

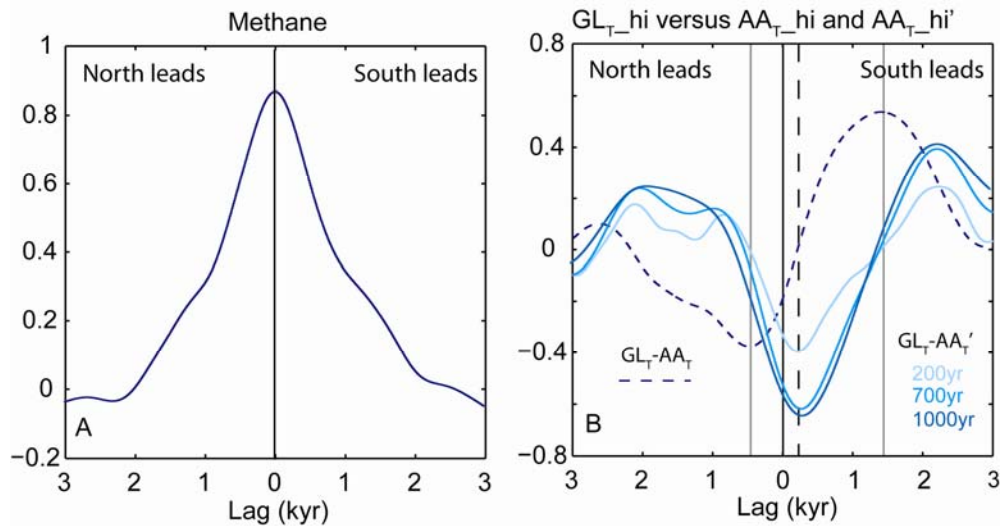


Figure S4. Cross correlations between records from the GISP 2 and Byrd ice cores as aligned by Blunier and Brook (4). (A) Methane correlation suggests that the tuning for gas phases is successful. (B) GL_T_{hi} versus AA_T_{hi} reveals the classic northern lead for an anti-correlation and southern lead for a positive correlation (5, 33). This may be contrasted with GL_T_{hi} versus AA_T_{hi}' , which show an anti-correlation with approximately zero phase (the apparent \sim 200 year lead of AA_T_{hi}' over GL_T_{hi} is within the uncertainty in Δ age). We find that an initial smooth of AA_T of 700 years (using a running mean, applied twice) gives optimal correlation with GL_T_{hi} whilst maintaining maximum detail in the derived record of AA_T_{hi}' (see also Fig. S2).

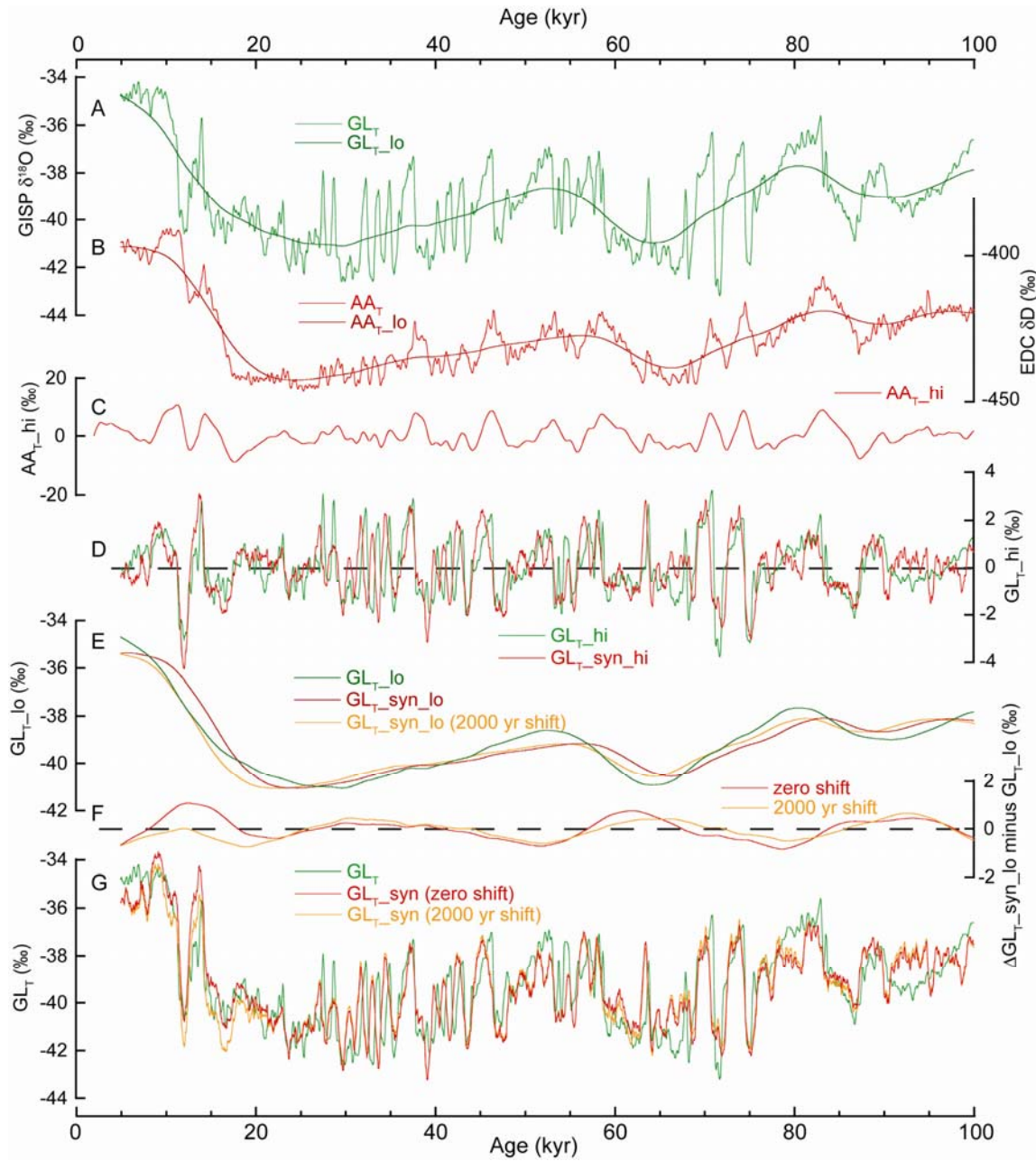


Figure S5. Construction of GL_T -syn. (A, B) the records of GL_T and AA_T respectively, with their orbital-timescale components, GL_T _lo and AA_T _lo. (C) the millennial-scale component of AA_T (AA_T _hi). (D) GL_T -syn_hi with GL_T -hi. (E) The orbital-timescale components, including a 2000 year shift of the Antarctic record. (F) Offsets between AA_T _lo and GL_T _lo with and without a 2000 year shift. (G) GL_T -syn (with and without a 2000 year shift) compared with GL_T .

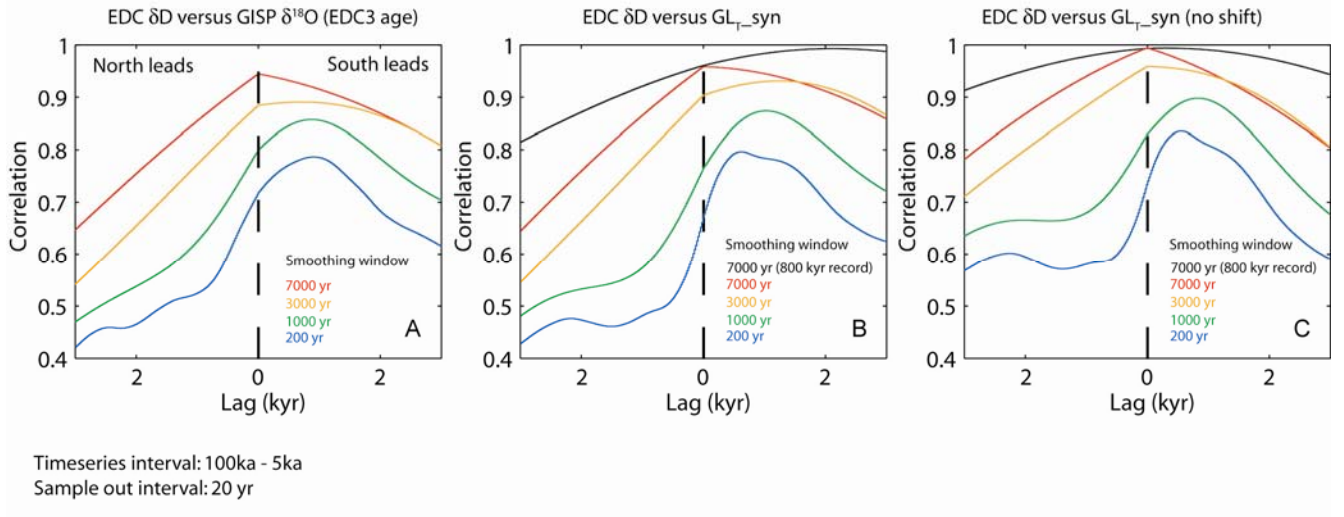


Figure S6. Lead lag correlations between GL_T and AA_T . (A) EDC δD versus GISP $\delta^{18}\text{O}$ for the interval 100 to 5 ka. A clear southern lead is observed for low order (200-1000 yr) smoothing of the records. The orbital-timescale components (7000 yr smooth; red curve) are highly correlated but the Greenland record is too short to allow a confident assessment of the relative phasing (maximum correlation is actually observed at zero lag but this is probably an artefact of the short record length relative to the smoothing window). (B) EDC δD versus $GL_T\text{-syn}$. In this case $GL_T\text{-syn}$ is produced by adding $GL_T\text{-syn_hi}$ to the scaled orbital-timescale component of AA_T ($AA_T\text{-lo}$) which has been shifted by 2000 years. The results for the interval 100 to 5 ka are very similar to panel (A) but now the records are long enough (~800 kyr; black curve) to allow observation of the 2000 year lag between the orbital components (a correlation of ~1 is obtained at a 2000 year lead of EDC δD over $GL_T\text{-syn}$). (C) EDC δD versus $GL_T\text{-syn}$ where the orbital-timescale component of $GL_T\text{-syn}$ has not been shifted. As expected, the correlation between the orbital-timescale components is a maximum at zero lag (black curve). Note also that for the interval 100 to 5 ka (red curve) the correlation is approximately symmetric about zero. This contrasts with the equivalent correlations in (A) and (B). We use this observation to support our inference that the orbital-timescale component of GISP $\delta^{18}\text{O}$ lags that of EDC δD by approximately 2000 years.

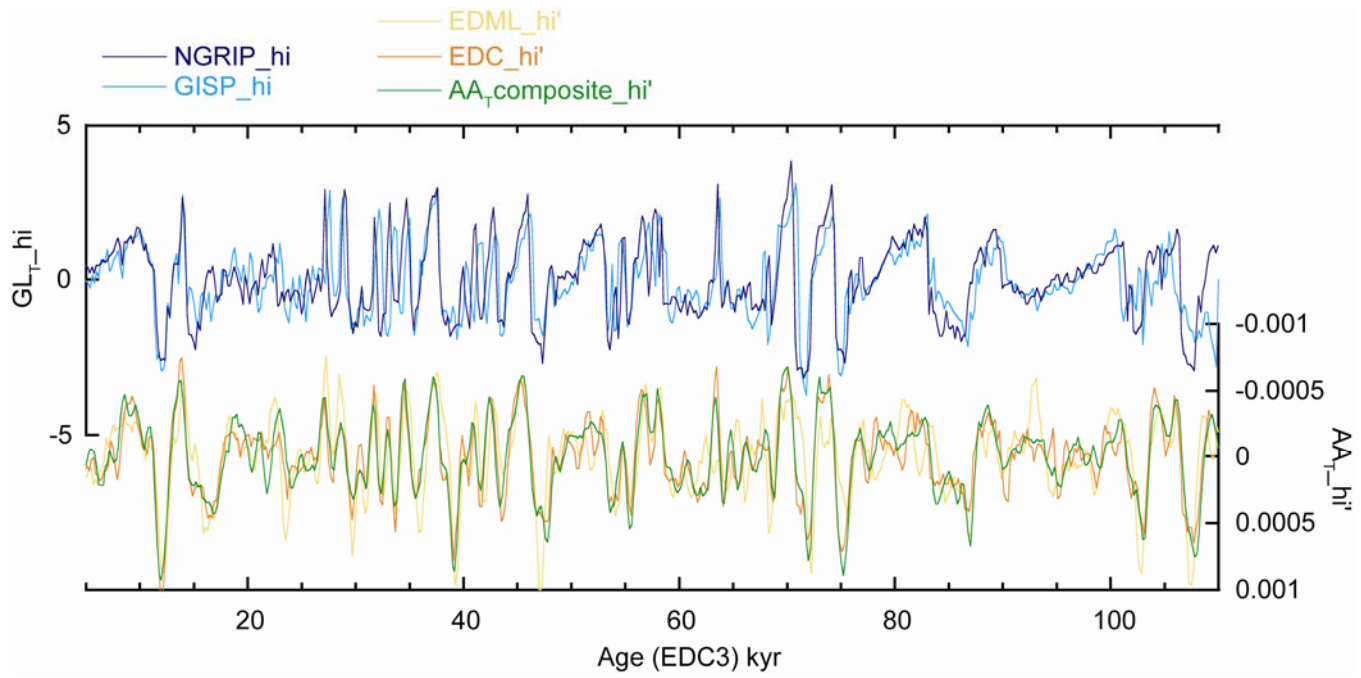


Figure S7. Comparison of the first differentials of EDC, EDML and a composite Antarctic record (derived by tuning and normalising the isotope records from EDC (8), EDML (17), Vostok (11), Dome Fuji (18) and Byrd (19)) with the millennial-scale components of the GISP (20) and NGRIP (21) ice cores. All records are on the EDC3 timescale. The GISP record was tuned via CH₄ (Fig. 1) and the NGRIP $\delta^{18}\text{O}$ record was tuned directly to GL_T-syn.

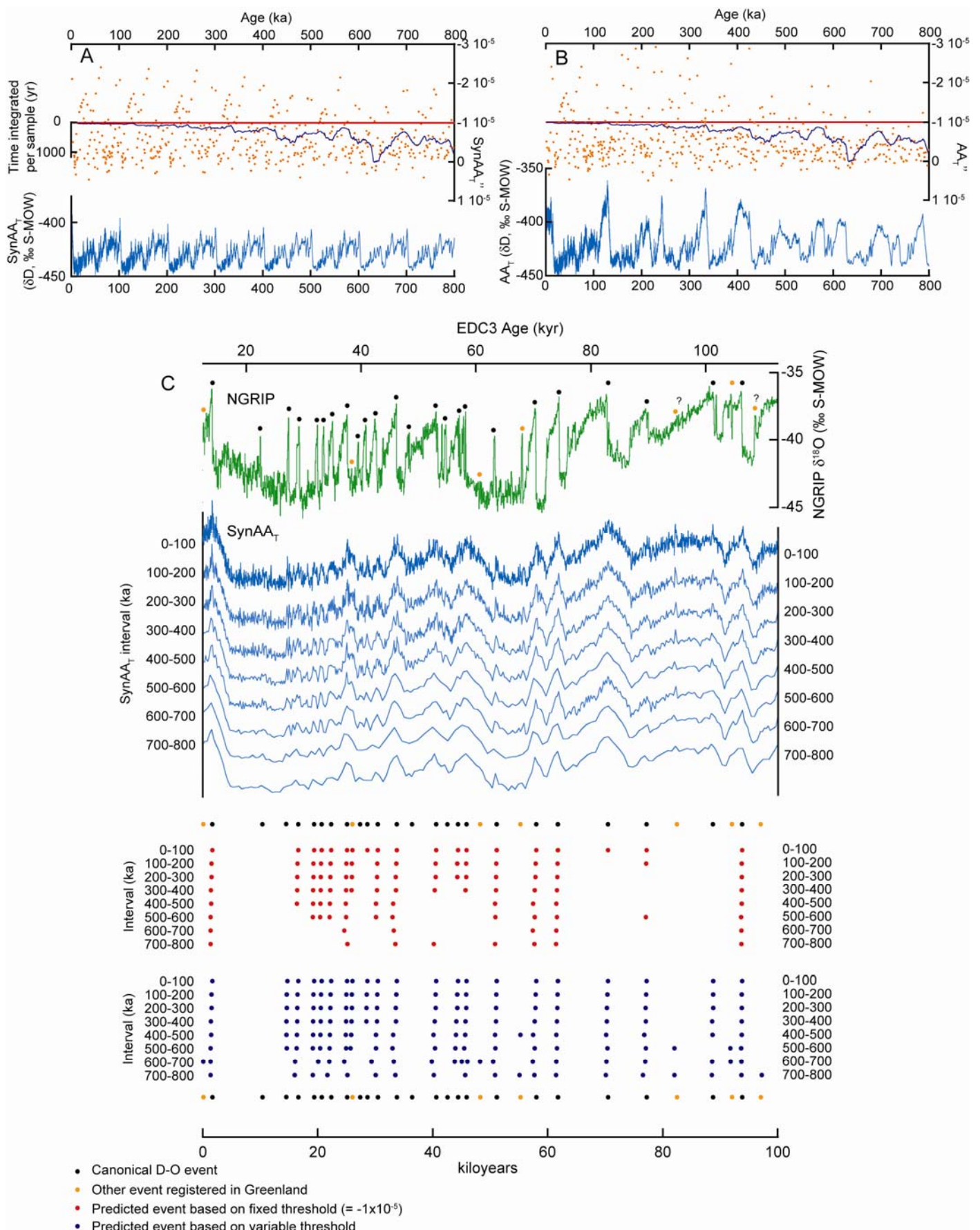


Figure S8. Accounting for signal attenuation using a synthetic ice core record. Panels (A) and (B) show the synthetic (A) and real (B) records of δD (light blue curves) for the last 800 kyr. For each record, the second differential (AA_T'') was calculated and the minima from each record are plotted as orange dots. With no loss of fidelity we would expect the minima in $SynAA_T''$ (the second

differential of the synthetic record) to be repeated for each 100 kyr section of the record and this can clearly be seen for the upper 400 kyr. Thus we would expect to be able to pick the same D-O events for each repeated interval. However, increasing time-per-sample (integrated time per 55cm sample of ice) in deeper sections of the core (dark blue curves in A and B) causes a decrease in the amplitude of δD variability and a corresponding decrease in the amplitude of AA_T'' variability. This is revealed by a general reduction in the minimum values for deeper sections and means that many events would be missed if a fixed threshold (red line) was applied (red dots in panel C). We therefore allow the threshold to vary according to the time-per-sample (the variable threshold is the same dark blue curve as represents time-per-sample but its Y-axis is the same as that for AA_T''). (C) The synthetic ice core record is now used to assess the success of the variable threshold. The red dots in panel C are the picked D-O events using a fixed threshold. More and more events are lost with each progressive 100 kyr interval, reflecting the loss of fidelity in the record. The same should be expected if using the real δD record from EDC. By using a varying threshold most of the events identified for the upper sections can also be selected for deeper sections (blue dots in panel C). The same varying threshold is then used to predict the occurrence of D-O events for the real record of δD (main text Figs. 3, 4). The record of $\delta^{18}O$ from NGRIP (21) shown here has been tuned to our record of GL_{T_syn} (on the EDC3 timescale) in order to allow comparison between predicted versus canonical (plus other) events (recall that the synthetic record is a repeat of the EDC3 interval 12–112 ka).

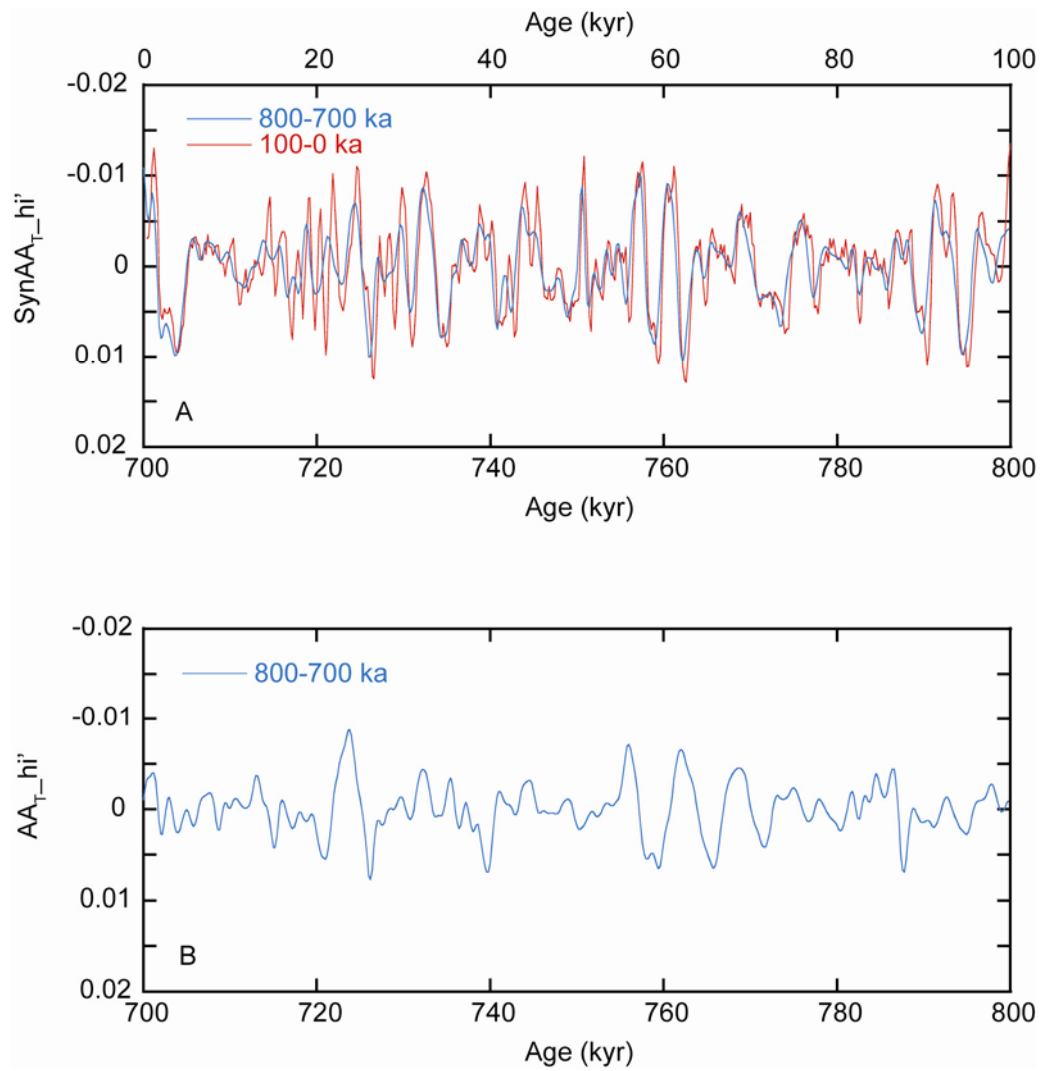


Figure S9. (A) Using the synthetic ice core record we can see that for shorter events (1-2 kyr) the increase in time-per-sample for deeper core sections results in a reduction in the amplitude of $\text{AA}_{\text{T_hi}'}$ and total loss of some events. However, for long events (e.g. those during terminations) there is minimal reduction in the amplitude of $\text{AA}_{\text{T_hi}'}$. (B) Based on this we argue that there should be minimal loss of amplitude in $\text{AA}_{\text{T_hi}'}$ for longer events in the deeper sections of the actual EDC δD record.

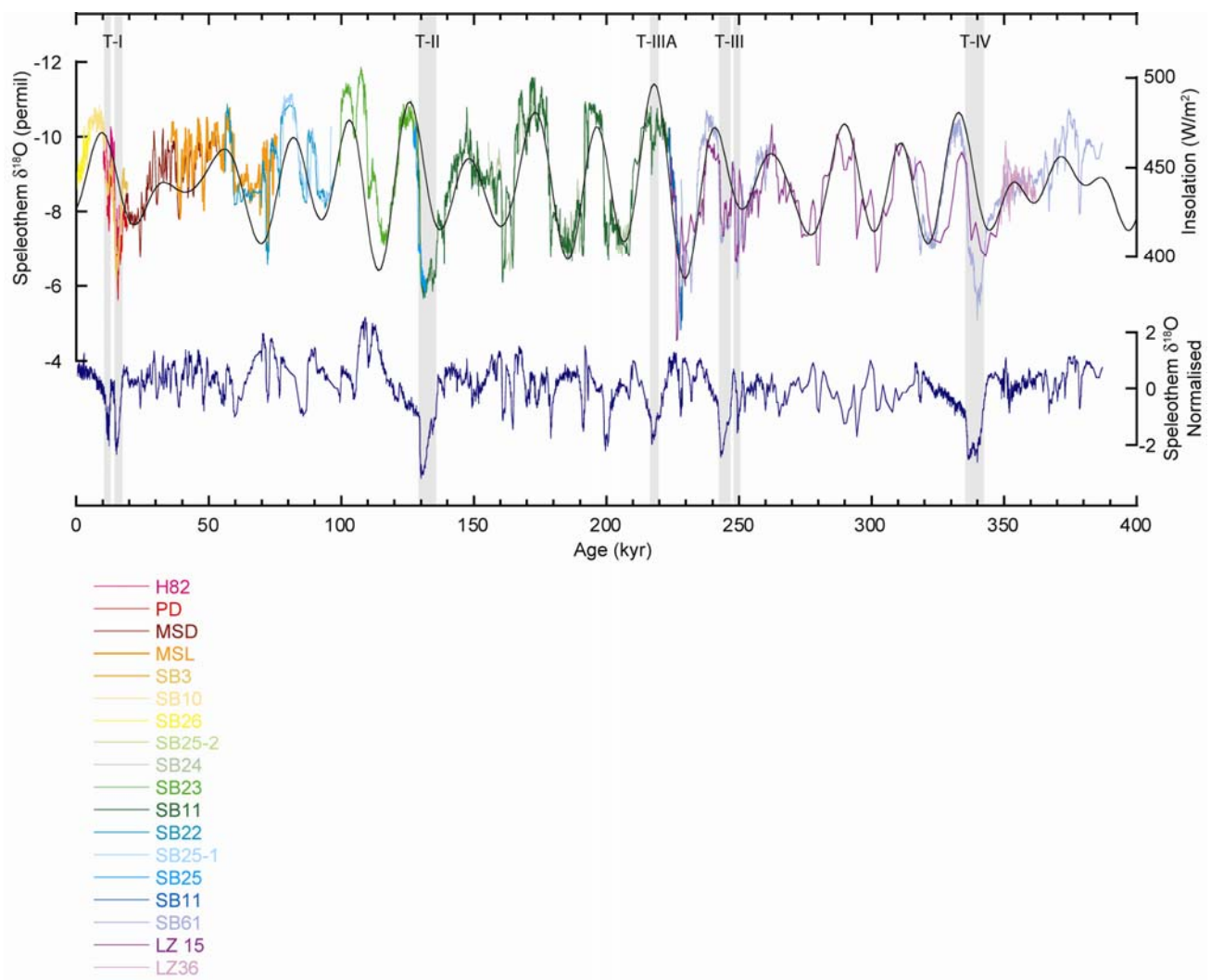


Figure S10. Normalisation of the Chinese speleothem record (24, 31, 32) to the record of insolation for July 21 at 65°N (34) highlights the nature of millennial-scale variability within this record.

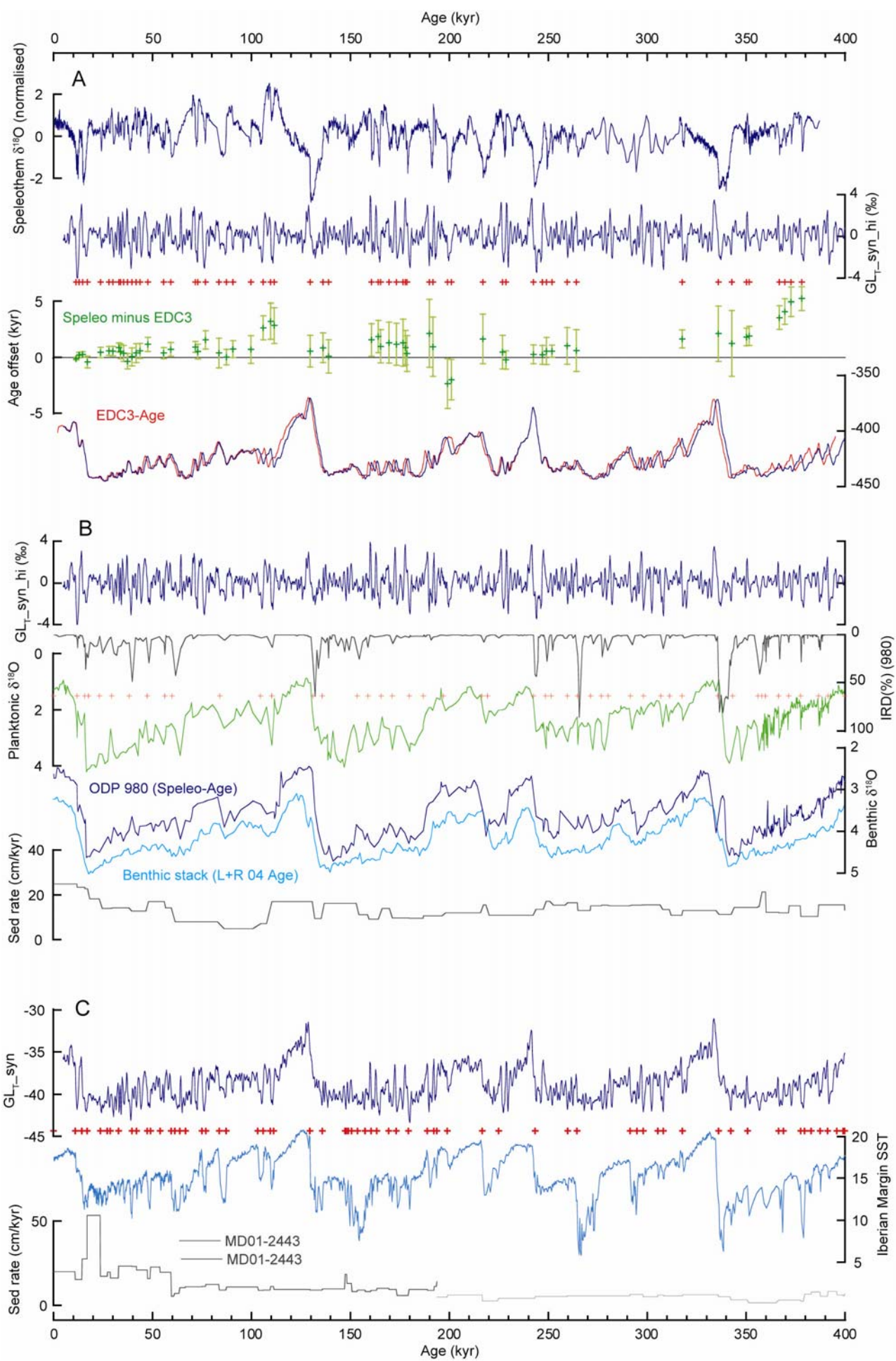


Figure S11 (previous page). (A) Tuning GL_T _syn_hi to the detrended speleothem record. Tuning points are indicated by red crosses. The deviation of our age model ('Speleo-Age') from the published EDC3 age model (27) is generally less than ~2kyr. Error bars are total estimated uncertainty in our absolute age points. (B) Tuning ODP 980 to GL_T _syn_hi (and GL_T _syn) via the records of planktonic foraminiferal $\delta^{18}O$ and %IRD(28) (red crosses are tuning points). The corresponding record of benthic $\delta^{18}O$ from the same core (on our new timescale) shows good correspondence with the benthic $\delta^{18}O$ stack published by (35). Also shown is the implied sedimentation rates for ODP 980. (C) The alkenone record of Iberian Margin SST (29) tuned to our record of GL_T _syn.

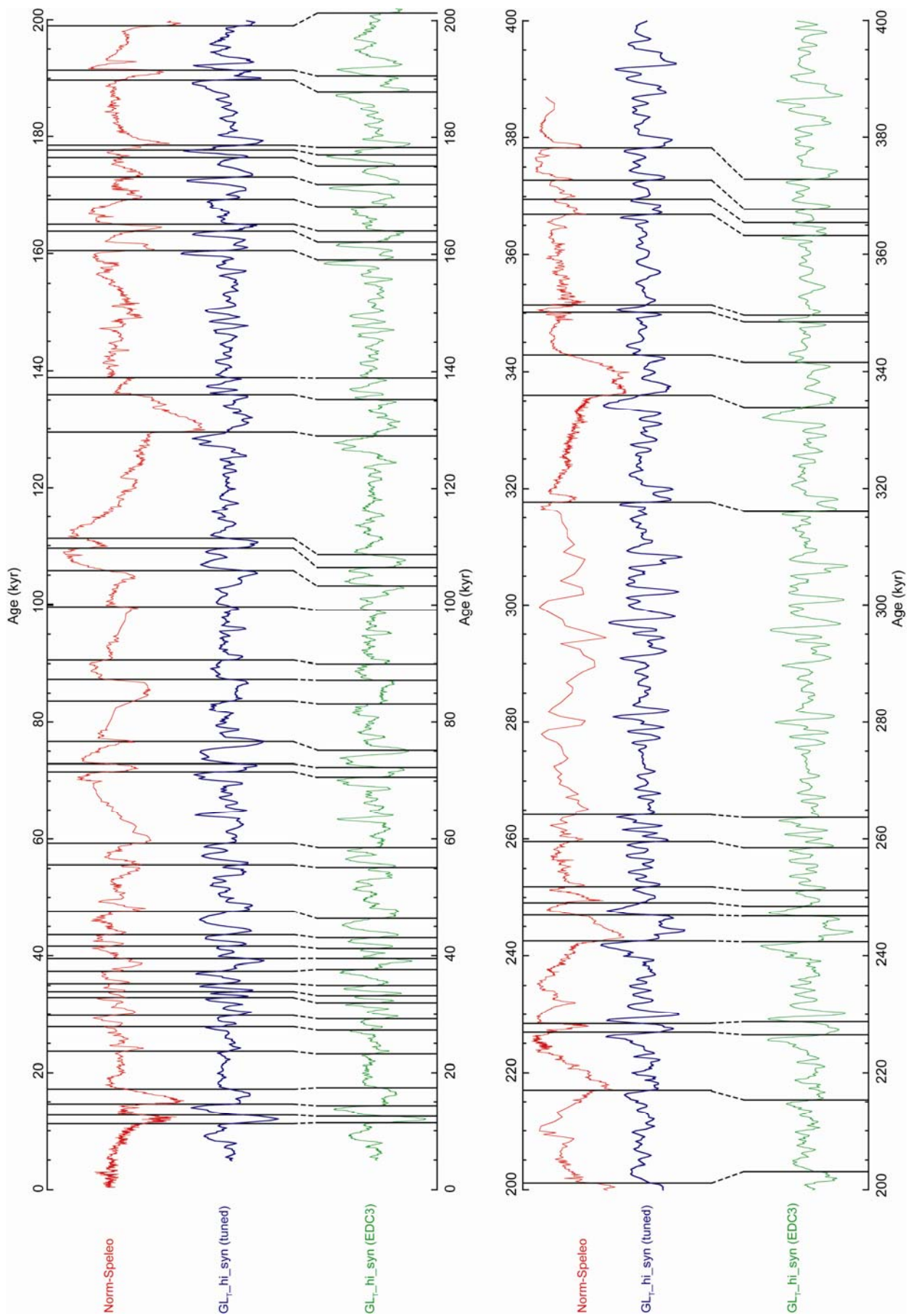


Figure S12. Detail of tuning between GL_T_syn_hi and the normalised speleothem record. No attempt is made to tune within the interval ~315 to 265 kyr, due to the lower resolution of the speleothem record at this time. Tuning points are given in Table S1.

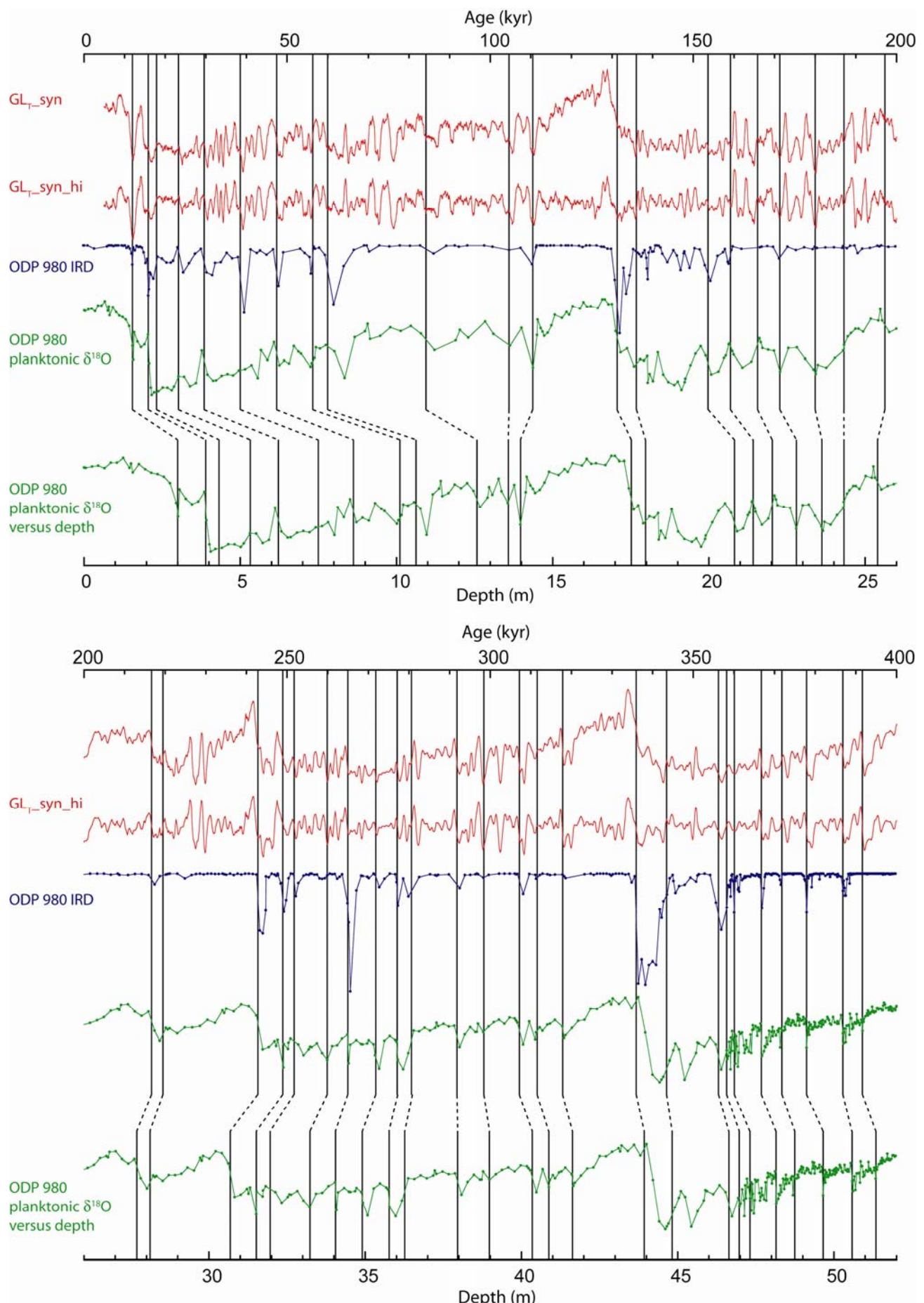


Figure S13. Detail of the tuning between ODP 980 (28) and GL_T_syn. Note that the records of both %IRD and planktonic foraminiferal $\delta^{18}\text{O}$ from ODP 980 were used for this exercise.

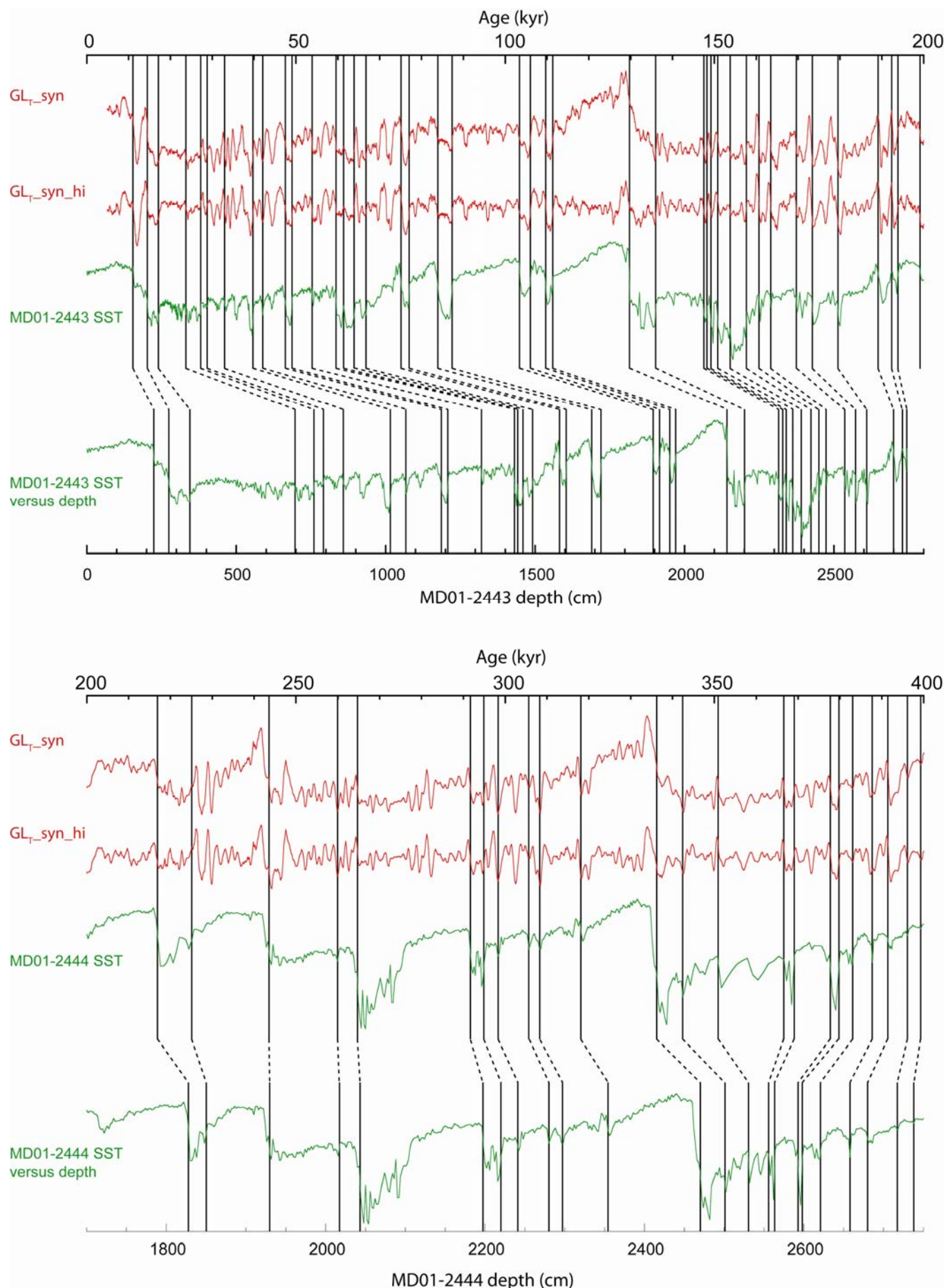


Figure S14. Detail of the tuning between the Iberian Margin SST record (29) and GL_T_syn

EDC3 age (kyr)	SpeleoAge (kyr)	Dage (kyr)	Tuning error (kyr)	Absolute speleo error (kyr)	Combined uncertainty (kyr)
11.47	11.36	-0.11	0.11	0.08	0.14
12.58	12.80	0.22	0.22	0.10	0.24
14.34	14.62	0.27	0.21	0.10	0.23
17.52	17.11	-0.40	0.50	0.10	0.51
23.29	23.77	0.47	0.42	0.15	0.45
27.40	28.00	0.60	0.36	0.19	0.41
29.33	29.90	0.57	0.36	0.21	0.42
32.04	32.94	0.90	0.25	0.33	0.41
33.35	33.90	0.55	0.36	0.54	0.65
35.00	35.38	0.38	0.34	0.63	0.71
37.76	37.43	-0.33	0.25	0.63	0.68
39.50	39.58	0.07	0.34	0.73	0.80
41.30	41.70	0.40	0.42	0.73	0.84
43.13	43.72	0.60	0.36	0.55	0.66
46.42	47.60	1.17	0.22	0.59	0.63
55.20	55.60	0.40	0.22	0.45	0.50
58.58	59.30	0.72	0.36	0.50	0.62
70.70	71.63	0.94	0.28	0.40	0.49
72.40	72.93	0.53	0.42	0.50	0.66
75.18	76.75	1.57	0.50	0.65	0.82
83.20	83.60	0.40	1.08	0.75	1.31
87.32	87.35	0.04	0.34	0.60	0.69
89.93	90.67	0.75	0.36	0.65	0.74
99.06	99.77	0.71	0.58	1.10	1.24
103.31	105.97	2.65	0.50	0.95	1.07
106.52	109.76	3.24	0.35	1.55	1.59
108.69	111.54	2.85	0.54	1.50	1.59
129.00	129.57	0.57	0.67	1.25	1.42
135.22	136.09	0.87	0.42	1.25	1.32
138.93	139.03	0.10	0.32	1.45	1.48
159.09	160.67	1.57	0.42	1.40	1.46
162.18	164.05	1.88	0.50	1.35	1.44
164.22	165.22	1.00	0.47	1.40	1.48
168.21	169.53	1.33	0.28	1.80	1.82
172.07	173.25	1.18	0.50	1.80	1.87
175.20	176.53	1.33	0.86	1.90	2.09
177.00	177.88	0.88	0.28	1.50	1.53
178.30	178.65	0.35	0.57	1.50	1.60
187.84	189.98	2.14	1.52	2.60	3.01
190.72	191.69	0.97	0.50	2.60	2.65
201.40	199.06	-2.35	0.42	2.20	2.24
203.12	201.13	-1.99	0.61	1.70	1.81
215.32	216.97	1.66	0.54	2.15	2.22
226.41	226.90	0.49	1.39	0.55	1.50
228.75	228.54	-0.22	0.42	0.70	0.82
242.27	242.55	0.28	0.81	0.25	0.85
246.75	246.99	0.24	0.78	0.30	0.84
248.46	249.04	0.57	1.17	0.30	1.21
251.28	251.85	0.58	0.50	0.20	0.54
258.52	259.56	1.04	0.57	1.55	1.65
263.62	264.24	0.62	1.04	1.55	1.87
316.04	317.70	1.66	0.40	0.70	0.81
333.83	335.96	2.13	1.30	2.10	2.47
341.56	342.83	1.27	2.04	2.10	2.93
348.43	350.26	1.83	0.28	0.75	0.80
349.59	351.53	1.94	0.28	0.80	0.85
363.26	366.82	3.57	0.36	1.00	1.06
365.40	369.50	4.10	0.50	1.00	1.12
367.79	372.75	4.96	0.50	1.20	1.30
372.90	378.15	5.25	0.30	1.00	1.04

Table S1 Age control points for placing the EDC records on the absolute age scale of speleothem records. Tuning errors are estimated from the widths of the selected transitions. Absolute speleothem errors are calculated from the quoted errors given for the nearest dated samples bracketing the selected tie point in the speleothem record (24, 31, 32).